LAWRENCE
LIVERMORE
NATIONAL
LABORATORY

LLNL-CONF-405029

DENSITY-FUNCTIONAL STUDY OF Zr-BASED ACTINIDE ALLOYS

A. Landa, P. Soderlind, P. Turchi, L. Vitos, A. Ruban

June 30, 2008

Plutonium Futures "The Science" 2008
Dijon, France
July 7, 2008 through July 11, 2008

Disclaimer

Density-functional study of Zr-based actinide alloys

Alex Landa[1*], Per Söderlind[1], Patrice E.A. Turchi[1], L. Vitos[2], and A. Ruban[2]

[1]Lawrence Livermore National Laboratory, Livermore, CA 94551, USA

[2]Royal Institute of Technology, SE-10044 Stockholm, Sweden

Abstract

Density-functional formalism is applied to study the phase equilibria in the U-Zr system. The obtained ground-state properties of the γ (bcc) and δ (C32) phases are in good agreement with experimental data. The decomposition curve for the γ-based U-Zr solutions is calculated. We argue that stabilization of the δ-UZr_2 phase relative to the α-Zr (hcp) structure is due to an increase of the Zr *d*-band occupancy that occurs when U is alloyed with Zr.

Keywords: nuclear reactor materials, phase transitions, first principles.

[*] Corresponding author. Tel.: + 1 925 424 3523; fax: +1 925 422 2851. E-Mail address: landa1@llnl.gov

Introduction

Zr-based actinide alloys, particularly U-Pu-Zr, proved to be very promising fuels for liquid metal fast breeder reactors because of their advantage in view of superior performance, reactor safety, and fuel cycle economics [1]. The main goal of fast breeder reactors is to achieve a so-called "high burn-up" fissioning all types of transuranic elements thus providing an appropriate solution to spent fuel recycling and complete transmutation of long-lived minor actinides (Np, Am, and Cm), which results in creation of a closed nuclear fuel cycle with future disposition of the nuclear waste products in a single geological repository [2].

In spite of the renewed interest in the Zr-based actinide alloys from the practical view point, very little has been done to understand fundamental aspects of phase equilibria in these systems. It was established [3] that the U-Zr system is characterized by the complete solubility of the body centered cubic high-temperature phases, γ-U and β-Zr, that is usually referred to in phase diagrams by 'γ-phase' solid solutions. Below $T \approx 995$ K, these solutions separate into a relatively flat miscibility gap, which ranges from about 10 to 40 at. % of Zr, and spans about 30 K below the critical point. The intermediate δ-phase is formed on cooling from the γ-phase around UZr_2 stoichiometry with the homogeneity range from 63 to 82 at. % Zr [4].

Both γ- and δ- phases in the U-Zr system play an important role in metallurgical reactions that occur during the nuclear burn-up [5-7]. Diffusion data and thermodynamic properties of the U-Zr alloys are very important for understanding phenomena occurring in the fuel rods under irradiation. That is why in order to study redistribution of Zr in the

U-Zr fuel rod one should perform, as the first step, *ab initio* calculations of the decomposition curve for the γ-U-Zr system, and calculate its basic ground-state properties. In this paper we present results of these calculations.

Another remarkable feature of the U-Zr system is the δ-UZr_2 phase, which solidifies in a modified C32 (AlB_2)-type crystal structure. It is well known that the high-temperature Zr- or Ti-based solid solutions may transform into the so-called metastable ω-phase at low temperatures [8]. This phase can also be stabilized from the α (hcp) phase of Zr (Ti) under compression [8, 9]. According to the X-ray and high resolution neutron diffraction structure analysis of the UZr_2 compound [4, 10], Zr atom occupies the "Al" position (0, 0, 0) of the hexagonal cell in the (AlB_2)-type crystal structure and a random mixture of U and Zr atoms occupies the "B" positions (⅔, ⅓, ½) and (⅓, ⅔, ½). Akabori *et al*. [11] performed interdiffusion coefficients measurements in the δ-UZr_2 phase by means of an electron-probe micro-analyzer, and found them to be significantly smaller than those extrapolated from the γ-U-Zr solid solutions [7] to the δ-phase. Finally, Ogawa *et al.* [12] suggested that the δ-UZr_2 intermediate phase could be regarded as an ω-phase solid solution that is stabilized against the α-Zr (hcp) structure by addition of U due to increase of the Zr *d*-band occupancy. In this paper we present results of calculations of the ground-state properties of the δ-UZr_2 phase and verified the hypothesis of this stabilization suggested in Ref. [12].

In our calculations we employ three complementary computational techniques: (i) scalar-relativistic Green's function technique based on the Korringa-Kohn-Rostoker (KKR) method within the atomic-sphere approximation (ASA), (ii) the scalar-relativistic

exact muffin-tin orbital method (EMTO), and (iii) the all-electron full-potential linear muffin-tin orbital method (FPLMTO) that accounts for all relativistic effects.

2. Computational details

The calculations we have referred to as KKR-ASA are performed using the scalar relativistic (no spin-orbit coupling) Green's function technique based on the KKR method within the atomic-sphere approximation [13-16]. The calculations are performed for a basis set including valence *spdf* orbitals and the semi-core 6*p* states for uranium whereas the core states are recalculated at every iteration (soft-core approximation). For the electron exchange and correlation energy functional, the generalized gradient approximation (GGA) is adopted [17]. Integration over the Brillouin zone is performed using the special *k*-point technique [18]. The moments of the density of states, needed for the kinetic energy and valence charge density, are calculated by integrating Green's function over a complex energy contour. The equilibrium density of the U-Zr system is obtained from a Murnaghan [19] fit.

In order to treat compositional disorder the KKR-ASA method is combined with the coherent potential approximation (CPA) [20]. The ground-state properties of the random U-Zr alloys are obtained from KKR-ASA-CPA calculations with the Coulomb screening potential and energy [21-23]. The screening constants are determined from supercell calculations using locally self-consistent Green's function method (LSGF) [24]. The effective cluster interactions (ECI), used in Monte Carlo (MC) simulations, are obtained from the screened generalized-perturbation method (SGPM) [21, 22, 25].

Though the KKR-ASA formalism is well suited to treat close-packed structures it could produce a significant error when being applied to 'open' structures such as C32. That is why we use another Green's function technique, based on the EMTO formalism, in present calculations, which is not limited by geometrical restrictions imposed by the ASA.

The EMTO calculations are performed using scalar-relativistic Green's function technique based on the improved screened KKR method, where the one-electron potential is represented by optimized overlapping muffin-tin (OOMT) potential spheres [26, 27]. As an output of the EMTO calculations, one can determine self-consistent Green's function of the system and the complete, non-spherically symmetric charged density. Finally, the total energy is calculated using the full charge-density technique [28]. Like in the case of KKR-ASA calculations, GGA is used for the electron exchange and correlation approximation, EMTO is combined with the CPA for calculation of the total energy of chemically random alloy. Integrations over the Brillouin zone, complex energy contour, and the choice of the screening constants are identical to the KKR-ASA method.

For the elemental metals, the most accurate and fully relativistic calculations are performed using an all-electron approach where the relativistic effects, including spin-orbit coupling, are accounted for. Although unable to model disorder in the CPA sense it provides important information for the metals, and also serves to confirm the CPA calculations mentioned above. For this purpose we use a version of the FPLMTO [29-31]. The "full potential" in FPLMTO refers to the use of non-spherical contributions to the electron charge density and potential. This is accomplished by expanding the charge density and potential in cubic harmonics inside non-overlapping muffin-tin spheres and

in a Fourier series in the interstitial region. We use two energy tails associated with each basis orbital, and for U's semi-core *6s*, *6p* states and valence states (*7s*, *7p*, *6d*, and *5f*) these pairs are different. With this 'double basis' approach we use a total of six energy tail parameters and a total of 12 basis functions per atom. Spherical harmonic expansions are carried out up to l_{max}= 6 for the bases, potential, and charge density. As in the case of the KKR-ASA and EMTO methods, GGA is used for the electron exchange-correlation approximation. A special quasi-random structure (SQS) method was used to treat the compositional disorder within the FPLMTO formalism [32].

3. Ground-state properties and decomposition curve of the γ-U-Zr solid solutions

Figures 1 (a-c) show results of KKR-ASA calculations of the equilibrium volume, Grüneisen constant, heat of formation of the γ-U-Zr solid solutions, as well as the bulk modulus and Debye temperature. The lattice vibration effects are accounted for within the so-called Debye-Grüneisen quasi-harmonic model [33, 34] and here evaluated at 300 K. Both equilibrium volume and heat of formation of the γ-U-Zr solid solutions show a positive deviation from Vegard's law that agrees well with the existence of a miscibility gap in the U-Zr phase diagram. One should notice that calculated heats of mixing of the γ-U-Zr solid solutions are in excellent agreement with data extracted from the experimental phase diagram by the use of CALPHAD methodology [35], which indicates the robustness of the *ab initio* approach used in the present calculations. For comparison, we also show the heats of formation of the γ-U-Zr for the $U_{75}Zr_{25}$, $U_{50}Zr_{50}$, and $U_{25}Zr_{75}$ alloys calculated within FPLMTO-SQS technique.

We performed MC calculations of the decomposition curve for the γ-U-Zr solid solutions. The MC simulations are performed using the Metropolis algorithm [36] for a 1728-site simulation box (12•12•12) with periodic boundary conditions. Figure 2 displays the calculated temperature of decomposition of the γ-$U_{1-c}Zr_c$ alloys within the wide range of composition. This curve has a maximum that is located somewhere between 20 and 30 at. % of Zr. This maximum matches relatively well the location of the maximum on the experimental miscibility gap (~ 30 at. % Zr) also shown in the figure. One should mention that that the decomposition curve indicates only the temperature of the phase transformation but tells nothing about the composition of the phases formed as a result. This information could be only found from the miscibility gap.

4. Ground-state properties of the δ-UZr_2 compound

The C32 (AlB_2) structure has two non-equivalent types of sublattice with 3 atoms per unit cell: sublattices of "Al-" (one site) and "B-" (two sites) types. As we mentioned in the Introduction, it is now believed that in the δ-UZr_2 compound Zr atoms occupy the Al-type position (0, 0, 0) of the hexagonal cell, and a random mixture of U and Zr atoms occupies the B-type positions (⅔, ⅓, ½) and (⅓, ⅔, ½). To confirm that this arrangement is actually the ground-state configuration of the δ-UZr_2 compound, we performed EMTO calculations of the equilibrium lattice constant for three atomic configurations of the C32 structure: (i) random distribution of U and Zr atoms on each of the three sites (the $U_{⅓}Zr_{⅔}$ "disordered" alloy); (ii) "complete' ordering with U atoms occupying the Al-type sublattice and Zr atoms occupying the B-type sublattice; (iii) "partial" ordering that corresponds to experimental observation described in Introduction. Figure 3 shows the

total energy of the δ-UZr_2 compound as a function of the Wigner-Seitz radius. One can see that the two types of ordering, "complete" and "partial", are energetically favorable in comparison with the disordered configuration, however, the configuration (iii) is one that has the lowest total energy (the ground-state).

We have also calculated the enthalpy of formation of the δ-UZr_2 compound. We define this property as

$$\Delta H_f = E_{UZr_2}^{C32} - \left[\frac{1}{3}E_U^{\alpha} + \frac{2}{3}E_{Zr}^{\alpha}\right], \qquad (6)$$

where $E_{UZr_2}^{C32}$ is the energy of the δ-UZr_2 compound and E_U^{α} and E_{Zr}^{α} are the energies of α-U and α-Zr, respectively. Present calculations reveal $E_{UZr_2}^{C32}$ = - 6.29 kJ/mol that is in fair agreement with experimental measurements of - 4.0 kJ/mol at T = 298 K [38, 39].

5. Stability of the δ-phase in the U-Zr system

It is well established that under compression zirconium metal undergoes the following phase transformations: α-Zr (hcp) $\rightarrow$ ω-Zr (C32) $\rightarrow$ β-Zr (bcc) [8, 9, 40-42]. We performed FPLMTO calculations of the total energy of α-, ω-, and β-Zr phases as functions of atomic volume and results of these calculations are shown in Figure 4. According to the present calculations, the $\alpha \rightarrow \omega$ and $\omega \rightarrow \beta$ phase transitions in Zr take place at 33 and 268 kbar, respectively, which are in a good accord with experimental measurements (see Table). One should also notice the significant scattering of the experimental data, especially for the $\alpha \rightarrow \omega$ transition.

Figure 5 (a) shows the *s*-, *p*-, and *d*-band occupations in α-Zr as a function of the Wigner-Seitz radius (FPLMTO calculations). As the Wigner-Seitz radius decreases (e.g., with increase of pressure), the occupation of the *d*-band goes up due to a loss of the *s*- and *p*-band electrons. In Figure 5 (b) we show the structural-energy difference obtained from canonical bands [43] as a function of *d*-band filling. One can see that as soon as the Zr *d*-band occupation increases under compression, hcp gradually transforms, initially to C32, and then to bcc.

Next, we discuss the analogies with the U-Zr system. Figure 6 has two parts. The upper part shows how the *d*-band occupation of α-Zr changes under compression and the transition region (full black) spans betweens the lower and upper experimental bounds, 21 kbar and 85 kbar (see Table), of the $\alpha \rightarrow \omega$ transformation. The hatched patch of the upper part of the plot shows the pressure region of the certain ω-phase stability in pure Zr. The lower part of this plot shows how the *d*-band occupation changes as a function of an increase in U composition in the U-Zr system. The hatched part of this part of the plot spans within the range of the homogeneity of the δ-U-Zr phase (18 – 37 at. % U [4]). One can see that at the upper pressure border of the $\alpha \rightarrow \omega$ phase transition range in pure Zr (~ 85 kbar) its *d*-occupation almost reaches the same value as it has when composition of U, alloyed with α-Zr, reaches the value (~ 18 at. %, [4]) when the δ-UZr_2 phase starts to form. Thus the present calculations confirm the hypothesis of Ref. [12] according to which the stabilization of the δ-UZr_2 phase in the U-Zr system has the same origin as that of the ω-phase in pure zirconium under compression, namely, it is induced by an increase in *d*-band filling.

6. Conclusion

In the present paper *ab initio* results on equilibrium properties are obtained for U-Zr alloys to understand the effectiveness of *ab initio* methods in describing actinide alloys. Ground-state properties of γ-U-Z solid solutions and the δ-UZr_2 compound were calculated. Predicted temperature of decomposition of γ-U-Zr alloys is in a reasonable agreement with the γ-phase miscibility gap. Stabilization of the δ-UZr_2 phase in the U-Zr system is explained in terms of an increase in *d*-band occupancy by the addition of U to Zr. These *ab initio* results will be used to build a completely theoretical phase diagram that can be compared with experimental and CALPHAD phase diagrams. This will serve as a template to investigate a mixture of U and Pu with minor actinides for which experimental data are lacking.

Acknowledgements

This work was performed under the auspices of the US Department of Energy by Lawrence Livermore National Laboratory under contract DE-AC52-07NA27344.

References:

1. G.L. Hofman, L.C. Walters, T.H. Bauer, Progr. Nucl. Energy (1/2) (1997) 83-110.
2. D.D. Keiser, Jr., J.B. Kennedy, B.A. Hilton, S.L Hayes, JOM (1) (2008) 29-32.
3. T. Ogawa, T. Iwai, J. Less-Comm. Met. 170 (1991) 101-108.
4. M. Akabori, A. Itoh, T. Ogawa, F. Kobayashi, Y. Suzuki, J. Nucl. Mater. 188 (1992) 249-254.
5. T. Ogawa, T. Iwai, M. Kurata, J. Less-Comm. Met. 175 (1991) 59-69.

6. G.L. Hofman, S.L. Hayes, M.C. Petri, J. Nucl. Mater. 227 (1996) 277-286.
7. T. Ogawa, M. Akabori, A. Itoh, T. Ogawa, J. Nucl. Mater. 232 (1996) 125-130.
8. S.K. Sikka, Y.K. Vohra, R. Chidambaran, Prog. Mater. Sci. 27 (1982) 245-310.
9. H. Xia, A.L. Ruoff, Y.K. Vohra, Phys. Rev. B 44 (1991) 10374-10376.
10. M. Akabori, T. Ogawa, A. Itoh, Y. Morii, J. Phys.: Condensed Matter 7 (1995) 8249-8257.
11. M. Akabori, A. Itoh, T. Ogawa, T. Ogata, J. Alloys Comp. 271-273 (1998) 597-601.
12. T. Ogawa, J.K. Gibson, R.G. Haire, M.M. Gensini, M. Akabori, J. Nucl. Mater. 223 (1995) 67-71.
13. O. Gunnarson, O. Jepsen, O.K. Andersen, Phys. Rev B 27 (1983) 7144-7168.
14. I.A. Abrikosov, H.L. Skriver, Phys. Rev B 47 (1993) 16532-16541.
15. A.V. Ruban, H.L. Skriver, Comput. Mater. Sci. 15 (1999) 119-143.
16. N.E. Christensen, S. Satpathy, Phys. Rev. Lett. 55 (1985) 600-603.
17. J.P. Perdew, K. Burke, M. Ernzerhof, Phys. Rev. Lett. 77 (1996) 3865-3868.
18. D.J. Chadi, M.L. Cohen, Phys. Rev. B 8 (1973) 5747-5753; Phys. Rev B 39 (1989) 3168-3172.
19. F.D. Murnaghan, Proc. Natl. Acad. Sci. U.S.A. 30 (1944) 244-247.
20. J.S. Faulkner, Prog. Mater. Sci. 27 (1982) 1-187.
21. A.V. Ruban, H.L. Skriver, Phys. Rev. B 66 (2002) 02420-1-115.
22. A.V. Ruban, S.I. Simak, P.A. Korzhavyi, H.l. Skriver, Phys. Rev. B 66 (2002) 024202-1-12.

23. A.V. Ruban, S.I. Simak, S. Shallcross, H.L. Skriver, Phys. Rev. B 67 (2003) 214302-1-12.

24. I.A. Abrikosov, S.I. Simak, B. Johansson, A.V. Ruban, H.L. Skriver, Phys. Rev. B 56 (1997) 9319-9334.

25. A.V. Ruban, I.A. Abrikosov, Rep. Prog. Phys. 71 (2008) 046501-1-30.

26. L. Vitos, Phys. Rev B 64 (2001) 014107-1-11.

27. L. Vitos, Computational Quantum Mechanics for Materials Engineers: The EMTO Method and Application, Springer, London, 2007.

28. J. Kollar, L. Vitos, H.L. Skriver, in: H. Dreyssé (Ed.), Electronic Structure and Physical Properties of Solids: The Uses of the LMTO Method, Lecture Notes in Physics, Springer, Berlin, 2000, pp. 85-113.

29. J.M. Wills, B. Cooper, Phys. Rev. B 36 (1987) 3809-3823.

30. D.L. Price, B. Cooper, Phys. Rev. B 39 (1989) 4945-4957.

31. J.M. Wills, O. Erikkson, M. Alouani, D.L. Price, in: H. Dreyssé (Ed.), Electronic Structure and Physical Properties of Solids: The Uses of the LMTO Method, Lecture Notes in Physics, Springer, Berlin, 2000, pp.148-167.

32. A. Zunger, S.H. Wei, L.G. Ferreira, J.E. Bernard, Phys. Rev. Lett. 65 (1990) 353-356.

33. V.L. Moruzzi, J.F. Janak, K. Schwartz, Phys. Rev. B 37 (1988) 790-799.

34. P. Söderlind, L. Nordström, L. Yongming, B. Johansson, Phys. Rev B 42 (1990) 4544-4552.

35. P.E.A. Turchi, I.A. Abrikosov, B. Burton, S.G. Fries, G. Grimvall, L. Kauffman, P. Korzhavyi, V. Rao Manga, M. Ohno, A. Pisch, A. Scott, W. Zhang, CALPHAD 31 (2007) 4-27.
36. K. Binder, Application of the Monte Carlo Method in Statistical Physics, Springer, Berlin, 1987.
37. H. Okamoto, J. Phase Equilib. 14 (2) (1993) 267-268.
38. K. Nagarajan, R. Babu, C.K. Mathews, J. Nucl. Mat. 203 (1993) 221-223.
39. T. Ogawa, J. Nucl. Mat. 209 (1994) 107-108.
40. S.A. Ostanin, V.Yu. Trubisin, Phys. Rev. 57 (1998) 13485-13490.
41. Y. Akahama, M. Kobayashi, H. Kawanura, J. Phys. Soc. Jap. 60 (1991) 3211-3214.
42. C.W. Greeff, Modeling Simul. Mater. Sci. Eng. 13 (2005) 1015-1027.
43. H.L. Skriver, Phys. Rev. B 31 (1985) 1909-192

Captions

Figure 1. The bulk modulus and Debye temperature (a); the heat of formation (b); the atomic volume and Grüneisen constant (c) of the γ-U-Zr alloys.

Figure 2. Temperature of decomposition of the γ-U-Zr alloys. Experimental data on the miscibility gap are taken from Ref. [37].

Figure 3. The total energy of the δ-UZr_2 compound for (i) - (iii) configurations (see text) as a function of the Wigner-Seitz radius. The equilibrium energy of the "partially' order configuration is used as the reference point and is set equal to zero.

Figure 4. The total energy of hcp, C32, and bcc Zr as a function of the atomic volume.

Figure 5. The change in band occupations in Zr under compression (a); the energy difference obtained from canonical *d*-bands calculations as a function of *d*-band occupancy (b). The hcp phase is used as the reference point and is set equal to zero.

Figure 6. Comparison of *d*-band occupancy in α-Zr as a function of compression with *d*-band occupancy in the U-Zr alloys as a function of U concentration.

Table. Experimental and theoretical (FPLMTO) pressure of the $\alpha \rightarrow \omega$ and $\omega \rightarrow \beta$ phase transitions in Zr.

Source	$\alpha \rightarrow \omega$ transition (kbar)	Source	$\omega \rightarrow \beta$ transition (kbar)
Ref. [8]	21 - 60	Ref. [9]	320
Ref. [40]	33 - 67	Ref. [41]	330
Ref. [42]	23 - 85	Ref. [42]	240 - 310
FPLMTO	33	FPLMTO	268

Figures.

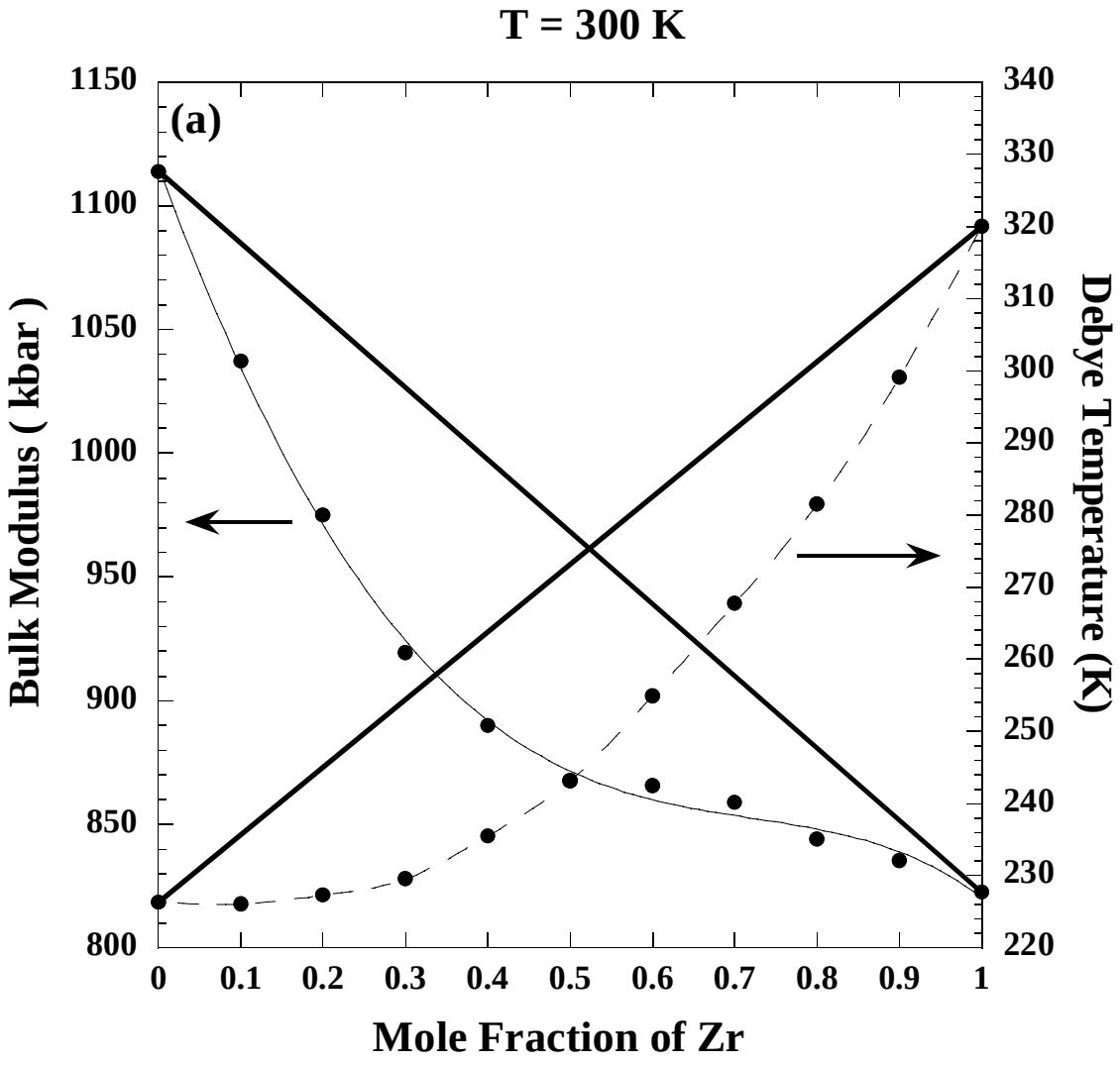

Figure 1a.

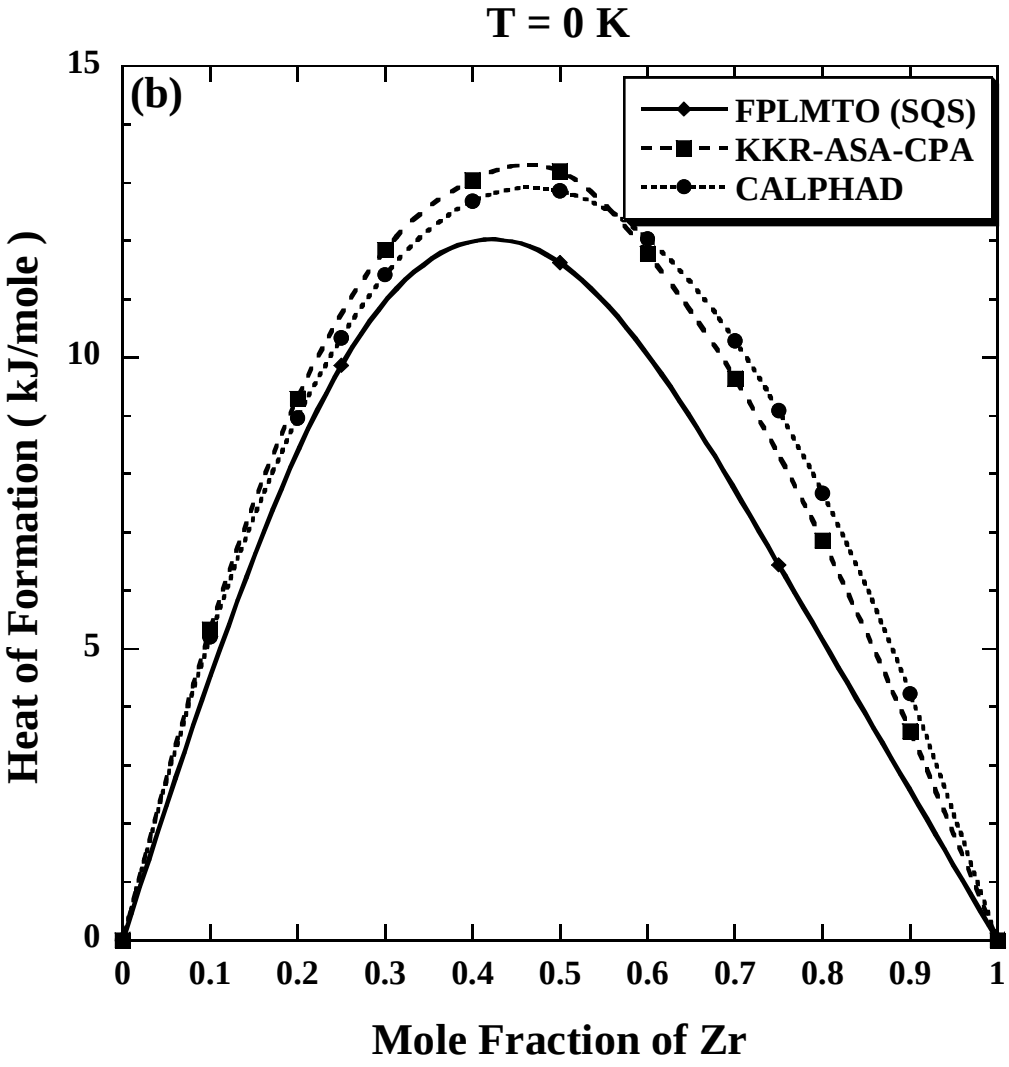
T = 0 K
(b)
FPLMTO (SQS)
KKR-ASA-CPA
CALPHAD
Heat of Formation (kJ/mole)
Mole Fraction of Zr
0
5
10
15
0
0.1
0.2
0.3
0.4
0.5
0.6
0.7
0.8
0.9
1

Figure 1 b.

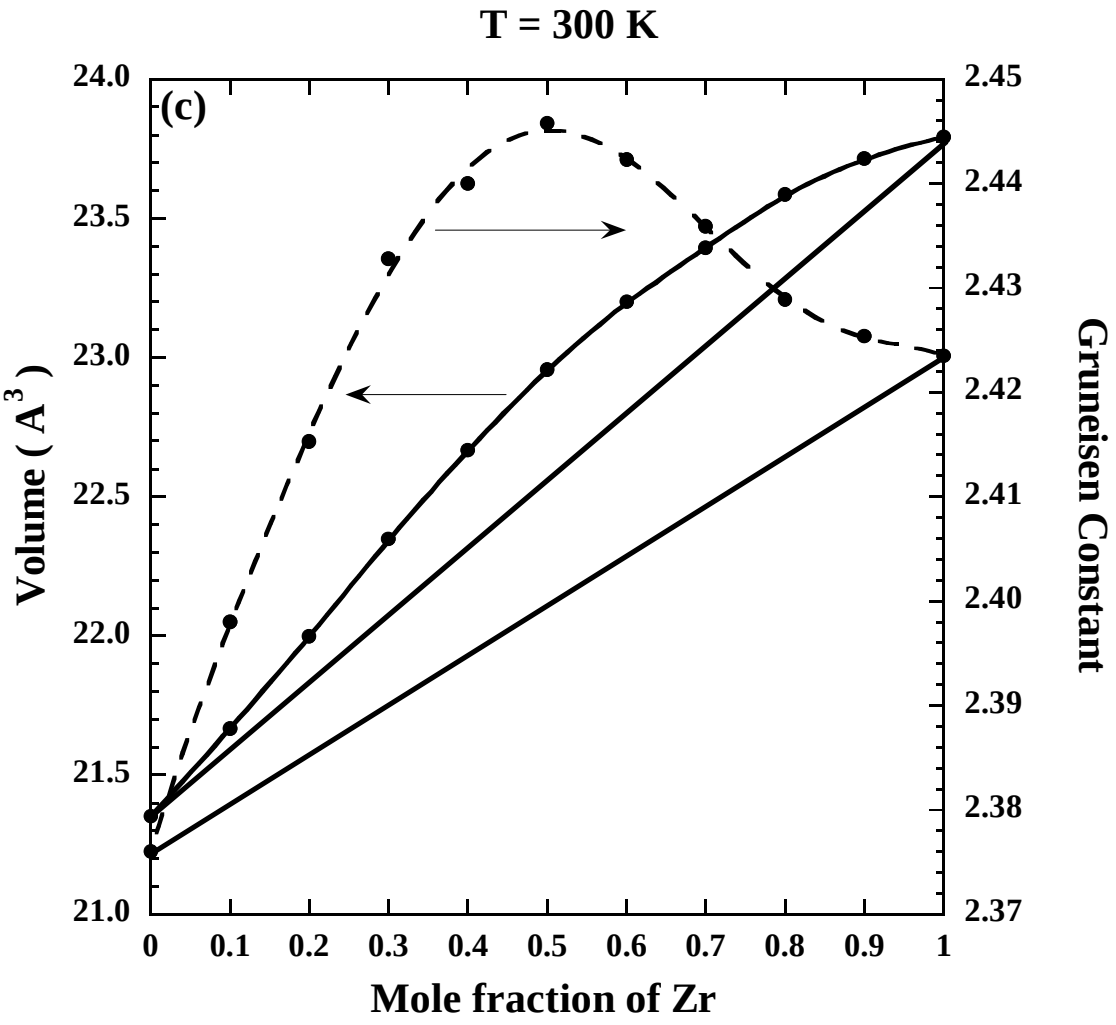
T = 300 K
(c)
Volume (A^3)
Gruneisen Constant
Mole fraction of Zr
24.0
23.5
23.0
22.5
22.0
21.5
21.0
2.45
2.44
2.43
2.42
2.41
2.40
2.39
2.38
2.37
0
0.1
0.2
0.3
0.4
0.5
0.6
0.7
0.8
0.9
1

Figure 1c.

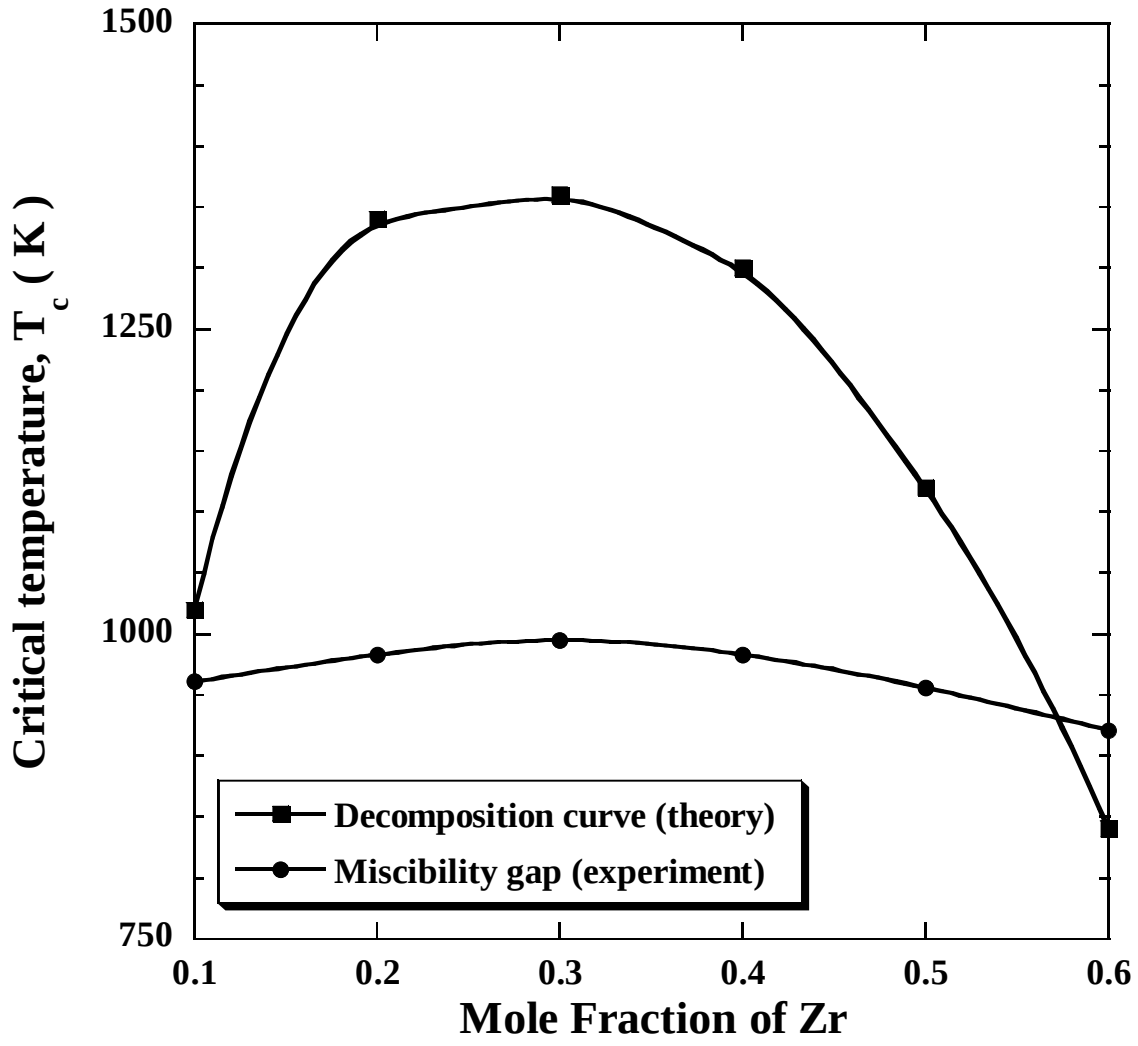
1500
1250
1000
750
Critical temperature, T_c (K)
0.1
0.2
0.3
0.4
0.5
0.6
Mole Fraction of Zr
Decomposition curve (theory)
Miscibility gap (experiment)

Figure 2.

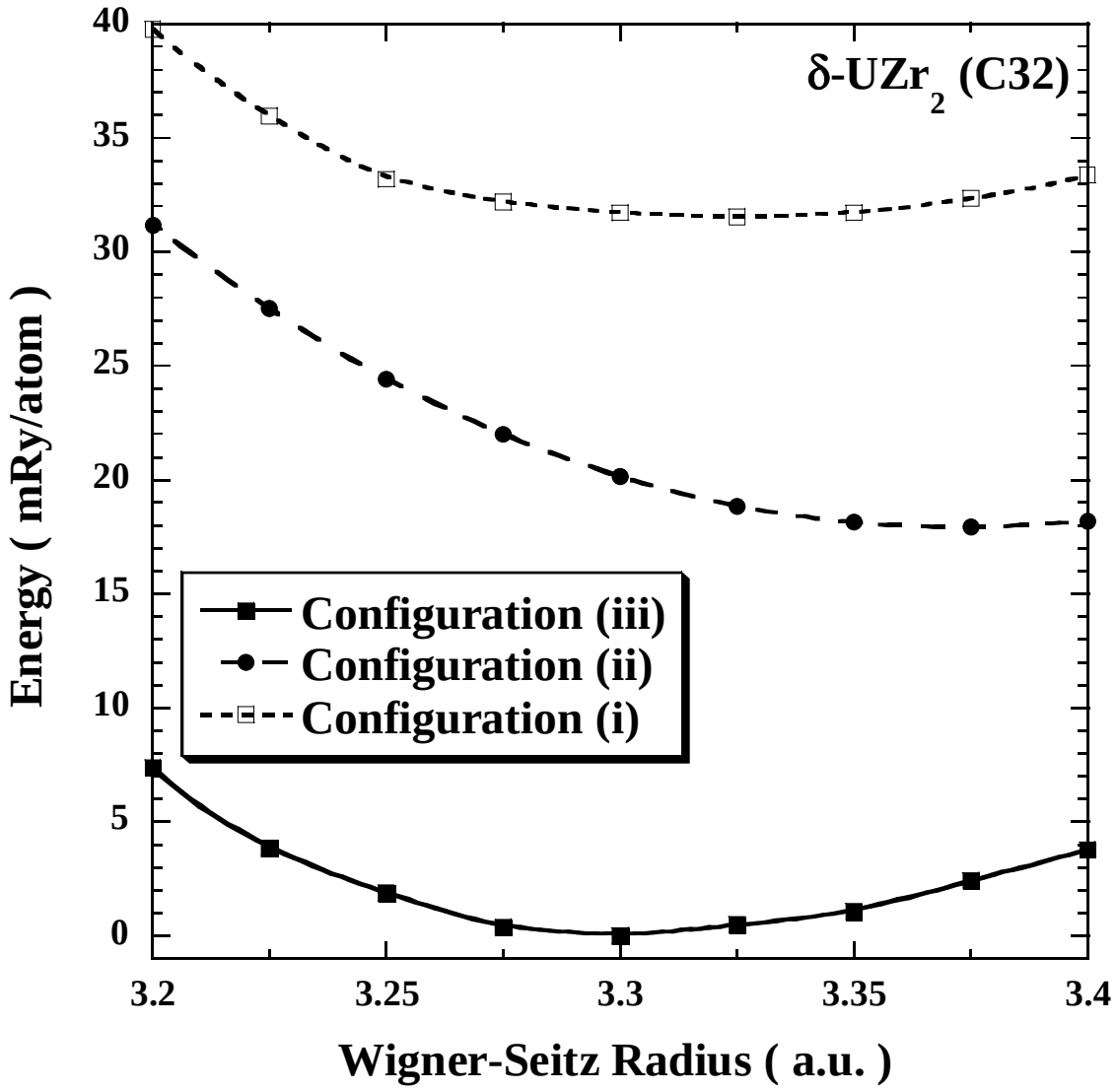
δ-UZr2 (C32)
Energy (mRy/atom)
Wigner-Seitz Radius (a.u.)
Configuration (iii)
Configuration (ii)
Configuration (i)
40
35
30
25
20
15
10
5
0
3.2
3.25
3.3
3.35
3.4

Figure 3.

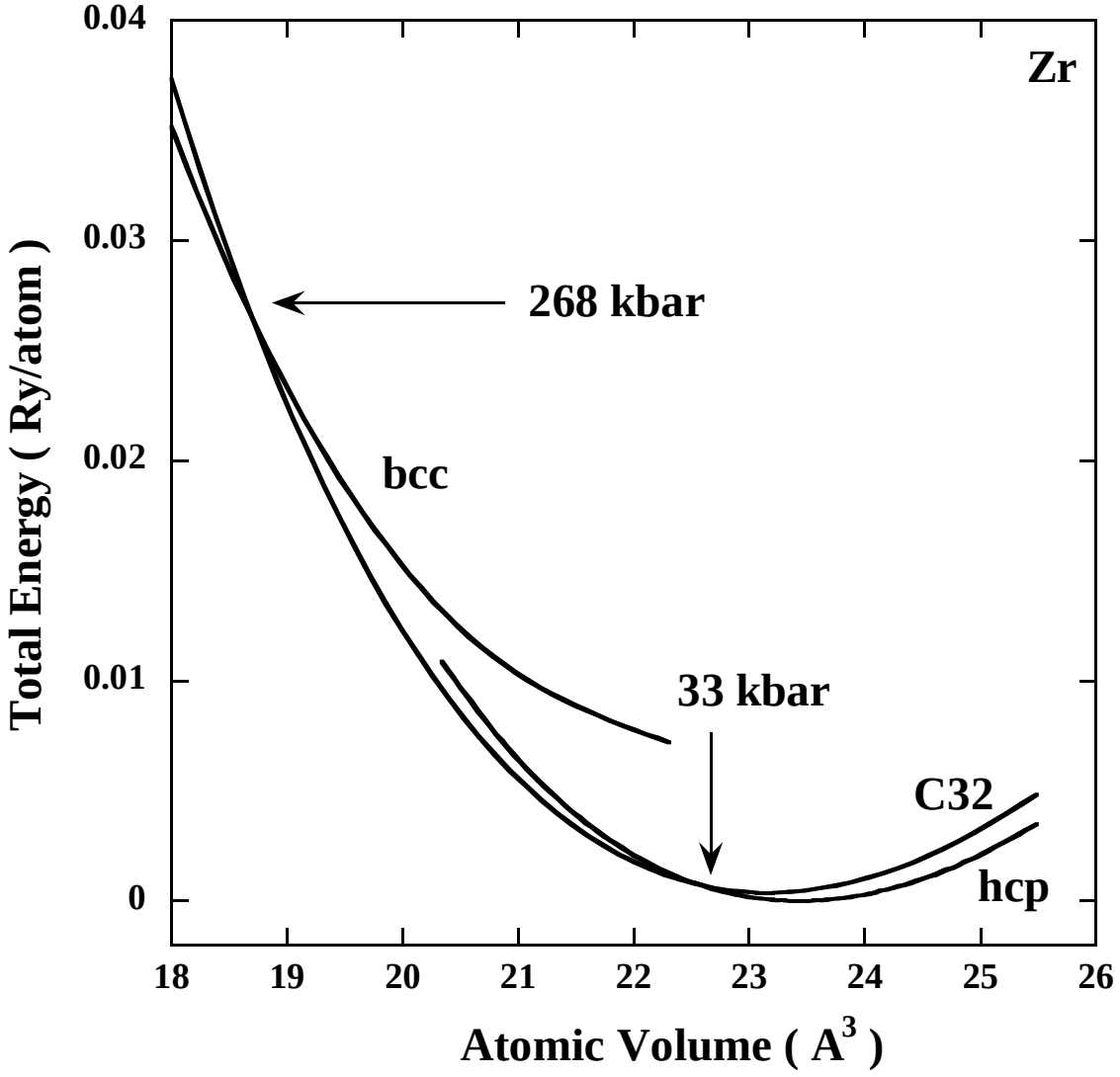
Zr
0.04
0.03
0.02
0.01
0
Total Energy (Ry/atom)
268 kbar
bcc
33 kbar
C32
hcp
18
19
20
21
22
23
24
25
26
Atomic Volume (A3)

Figure 4.

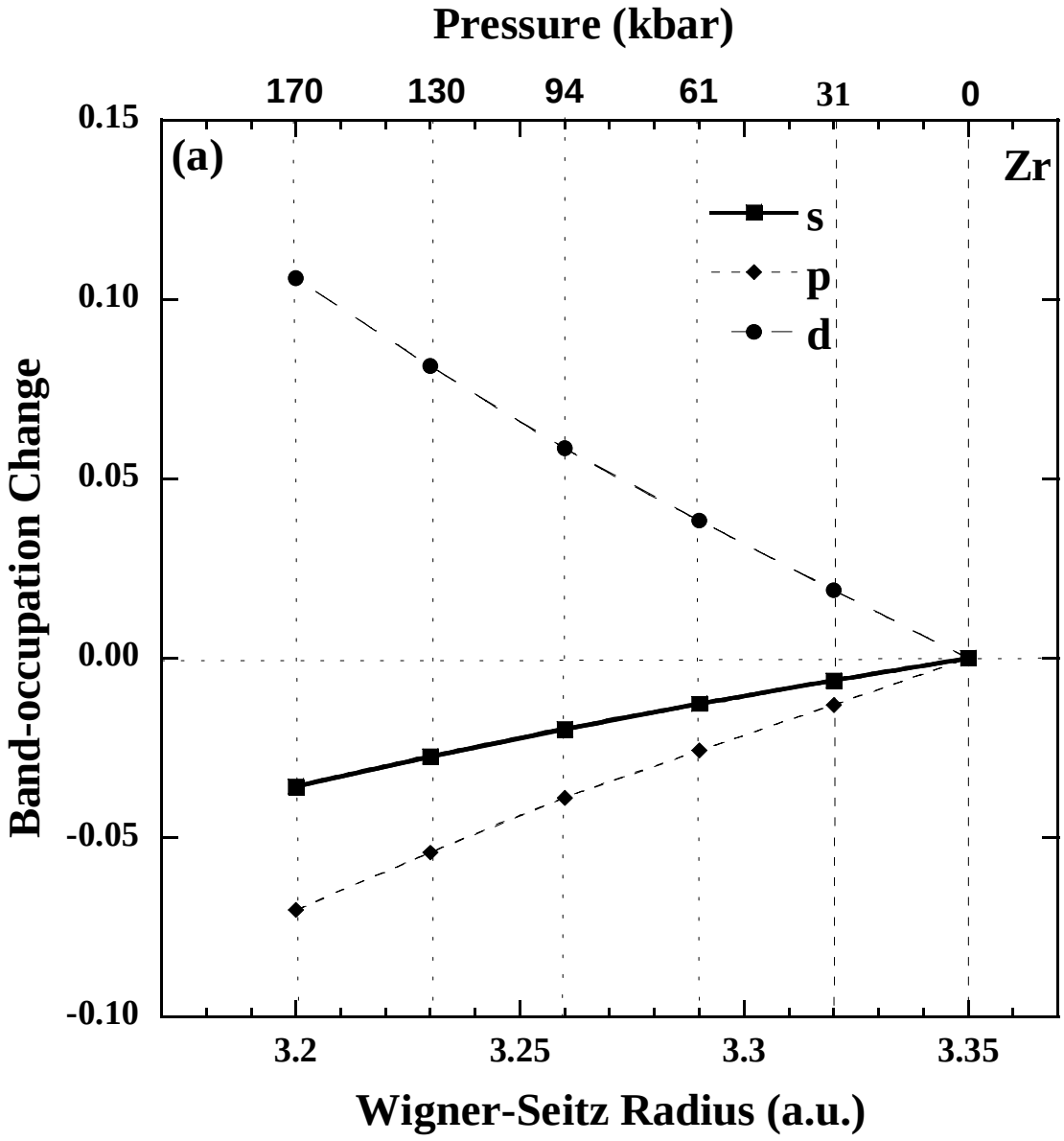
Pressure (kbar)
170
130
94
61
31
0
(a)
Zr
s
p
d
0.15
0.10
0.05
0.00
-0.05
-0.10
Band-occupation Change
3.2
3.25
3.3
3.35
Wigner-Seitz Radius (a.u.)

Figure 5 a.

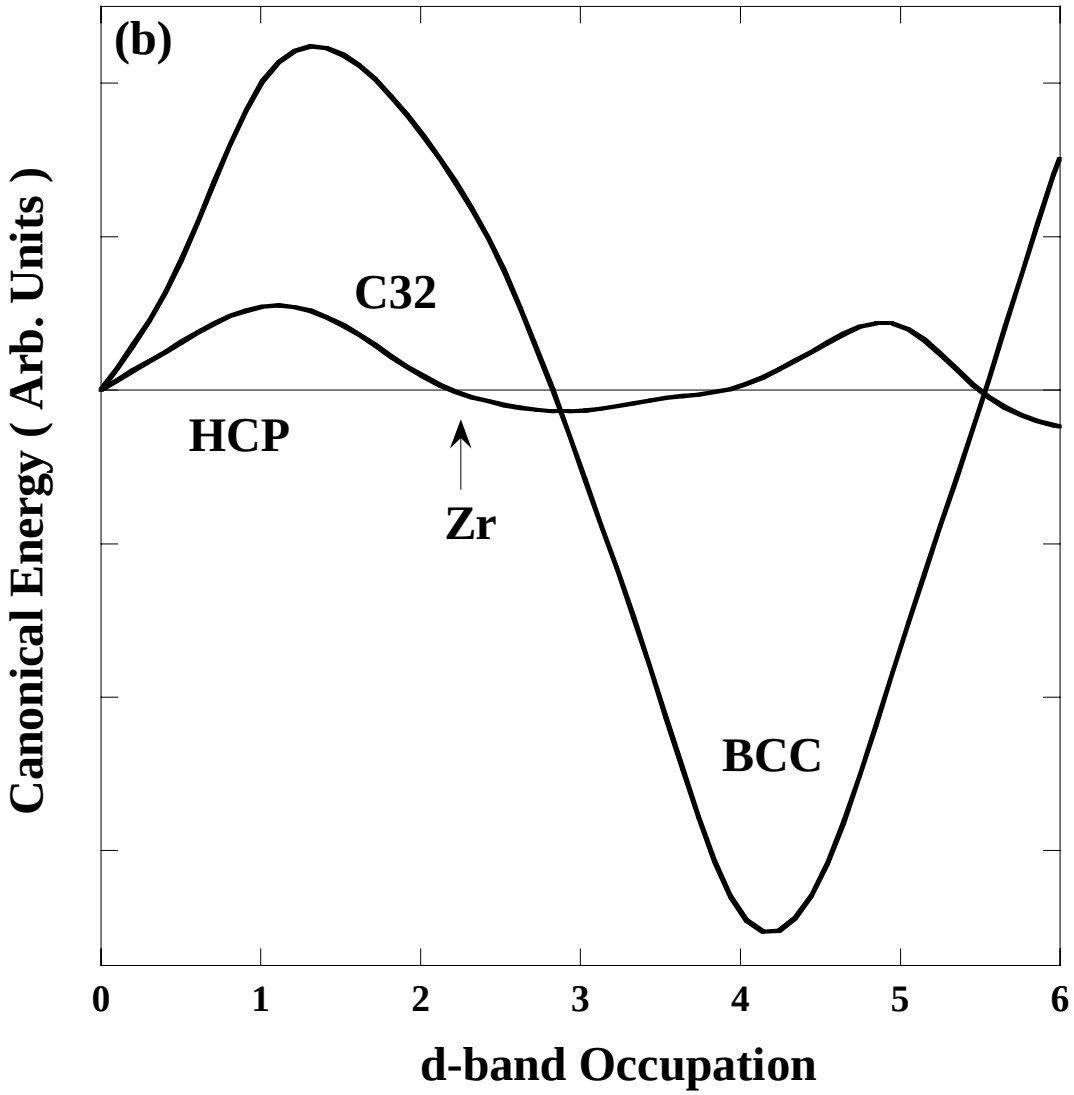
(b)
C32
HCP
Zr
BCC
Canonical Energy (Arb. Units)
0
1
2
3
4
5
6
d-band Occupation

Figure 5 b.

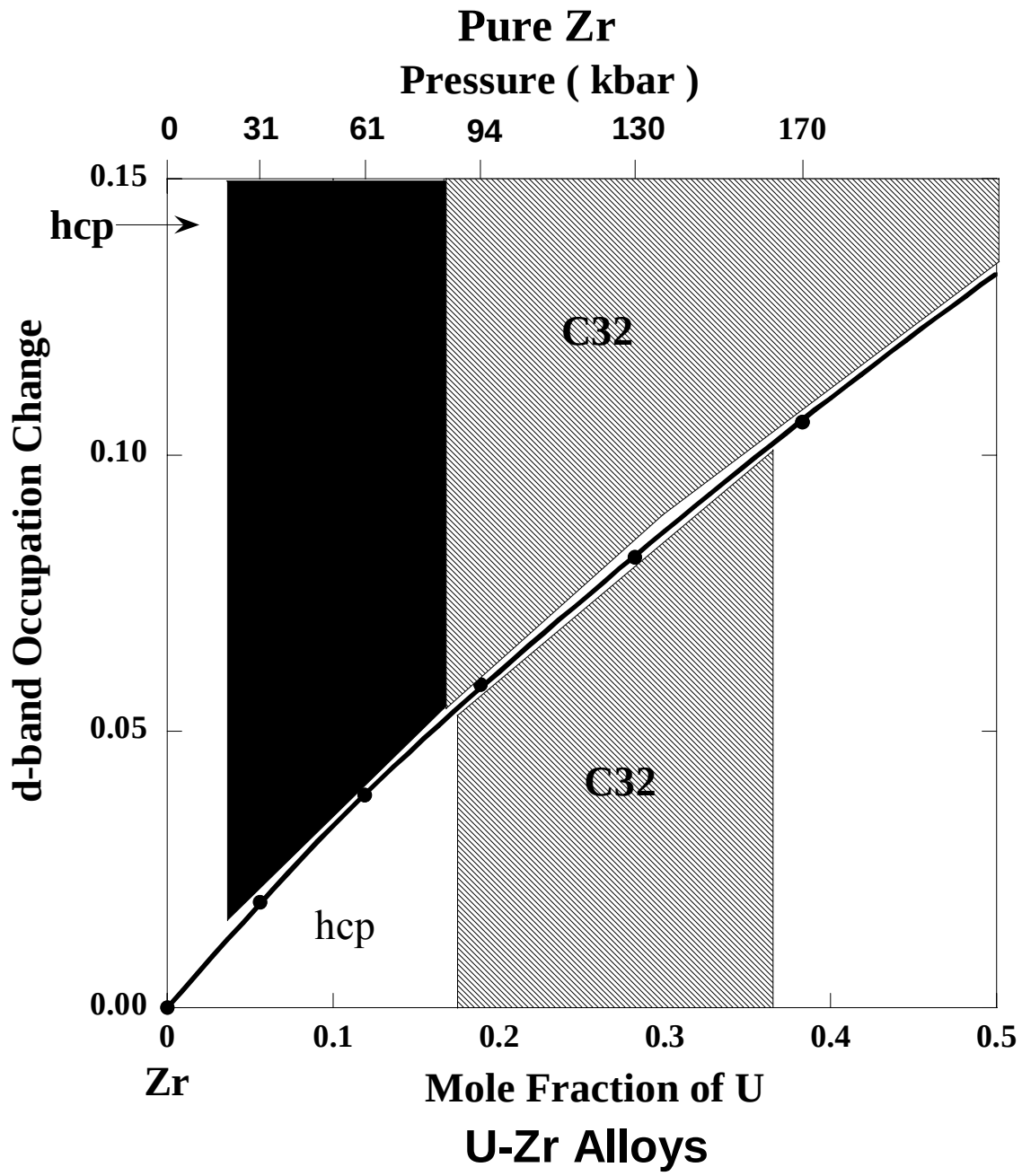
Pure Zr
Pressure (kbar)
0
31
61
94
130
170
0.15
hcp
0.10
0.05
0.00
d-band Occupation Change
C32
C32
hcp
0
0.1
0.2
0.3
0.4
0.5
Zr
Mole Fraction of U
U-Zr Alloys

Figure 6.